NUMERICAL LINEAR ALGEBRA WITH APPLICATIONS
Numer. Linear Algebra Appl. (2010)
Published online in Wiley Online Library (wileyonlinelibrary.com). DOI: 10.1002/nla.761

Robust multigrid preconditioners for the high-contrast biharmonic plate equation

Burak Aksoylu[1,2,*,†] and Zuhal Yeter[2]

[1]*Department of Mathematics, TOBB University of Economics and Technology, Ankara 06560, Turkey*
[2]*Department of Mathematics, Louisiana State University, Baton Rouge, LA 70803, U.S.A.*

SUMMARY

We study the high-contrast biharmonic plate equation with Hsieh–Clough–Tocher discretization. We construct a preconditioner that is robust with respect to contrast size and mesh size simultaneously based on the preconditioner proposed by Aksoylu *et al.* (*Comput. Vis. Sci.* 2008; **11**:319–331). By extending the devised singular perturbation analysis from linear finite element discretization to the above discretization, we prove and numerically demonstrate the robustness of the preconditioner. Therefore, we accomplish a desirable preconditioning design goal by using the same family of preconditioners to solve the elliptic family of PDEs with varying discretizations. We also present a strategy on how to generalize the proposed preconditioner to cover high-contrast elliptic PDEs of order $2k$, $k>2$. Moreover, we prove a fundamental qualitative property of the solution to the high-contrast biharmonic plate equation. Namely, the solution over the highly bending island becomes a linear polynomial asymptotically. The effectiveness of our preconditioner is largely due to the integration of this qualitative understanding of the underlying PDE into its construction.

Received 2 October 2009; Revised 23 September 2010; Accepted 12 October 2010

KEY WORDS: biharmonic equation; plate equation; fourth-order elliptic PDE; Schur complement; low-rank perturbation; singular perturbation analysis; high-contrast coefficients; discontinuous coefficients; heterogeneity

1. INTRODUCTION

We study the construction of robust preconditioners for the high-contrast biharmonic plate equation (also referred to as the biharmonic equation). Our aim is to achieve robustness with respect to the contrast size and the mesh size simultaneously, which we call as m- and h-robustness, respectively. In the case of a high-contrast diffusion equation, we studied the family of preconditioners B_{AGKS} by proving and numerically demonstrating that the same family used for finite element discretization [1] can also be used for conservative finite volume discretizations with minimal modification [2]. In this article, we extend the applicability of B_{AGKS} even further and show that the very same preconditioner can be used for a wider family of elliptic partial differential equations (PDEs). The broadness of the applicability of B_{AGKS} has been achieved by singular perturbation analysis (SPA) as it provides valuable insight into qualitative nature of the underlying PDE and its discretization. In order to study the robustness of B_{AGKS}, we use an SPA that is similar to the one devised on the matrix entries by Aksoylu *et al.* [1]. SPA turned out to be an effective tool in analyzing certain behaviors of the discretization matrix $K(m)$ such as the

*Correspondence to: Burak Aksoylu, Department of Mathematics, TOBB University of Economics and Technology, Ankara 06560, Turkey.
†E-mail: baksoylu@etu.edu.tr

asymptotic rank, decoupling, and low-rank perturbations (LRP) of the resulting submatrices. LRPs are exploited to accomplish dramatic computational savings and this is the main numerical linear algebra implication.

The devised SPA is utilized to explain the properties of the submatrices related to $K(m)$. In particular, SPA of highly bending block $K_{\mathrm{HH}}(m)$, as modulus of bending $m \to \infty$, has important implications for the behavior of the Schur complement $S(m)$ of $K_{\mathrm{HH}}(m)$ in $K(m)$. Namely,

$$S(m) := K_{\mathrm{LL}} - K_{\mathrm{LH}} K_{\mathrm{HH}}^{-1}(m) K_{\mathrm{HL}} = S_\infty + \mathcal{O}(m^{-1}), \tag{1}$$

where S_∞ is a LRP of K_{LL}. The rank of the perturbation depends on the number of disconnected components comprising the highly bending region. This special limiting form of $S(m)$ allows us to build a robust approximation of $S(m)^{-1}$ by merely using solvers for K_{LL} by the help of the Sherman–Morrison–Woodbury formula.

Preconditioning for the biharmonic equation was extensively studied in the domain decomposition setting [3, 4] and multigrid, BPX, and hierarchical basis settings [5–10]. Other solution strategies were also developed such as fast Poisson solvers [11, 12] and iterative methods [13]. However, there is only limited preconditioning literature available for discontinuous coefficients. Domain decomposition preconditioners have been studied [14] for the mortar-type discretization of the biharmonic equation with large jumps in the coefficients.

The high-contrast in material properties is ubiquitous in composite materials. Hence, the modeling of composite materials is an immediate application of the biharmonic plate equation with high-contrast coefficients. Since the usage of composite materials is steadily increasing, the simulation and modeling of composites have become essential. We witness that the utilization of composites has become an industry standard. For instance, lightweight composite materials are now being used in modern aircrafts by Airbus and Boeing. There is imminent need for robust preconditioning technology in the computational material science community as the modeling and simulation capability of composites evolve.

In [15], the Euler–Bernoulli equation with discontinuous coefficients was studied for the kinematics of composite beams. In the beam setting, the physical meaning of the PDE coefficient corresponds to the product of Young's modulus and moment of inertia [15] [16, p. 103]. In the biharmonic plate equation setting, the PDE coefficient represents the plate modulus of bending [16, p. 406]. Nonhomogeneous elastic plates have been considered in [17] with varying modulus of elasticity.

Our model problem is limited to the biharmonic equation that captures only the *isotropic* materials. The extension of our analysis to a more generalized fourth-order PDE is widely open. Such PDEs have an important role in structural mechanics as they are used in modeling *anisotropic* materials. Plane deformations of anisotropic materials were studied in [18], but extension to a simultaneously heterogeneous and anisotropic case needs to be further explored. Grossi [19] has studied the existence of the weak solutions of anisotropic plates. The coercivity of the bilinear forms has also been established, which may lay the foundations for our future work related to LRPs.

The remainder of the article is structured as follows. In Section 2, we present the underlying high-contrast biharmonic plate equation and the associated bilinear forms. Subsequently, the effects of high-contrast on the spectrum of stiffness matrix and its subblocks are also discussed. Since the proposed preconditioner is based on LRP, in Section 3, we study the LRP of the limiting Schur complement as in (1). In Section 4, we present the aforementioned SPA and reveal the asymptotic qualitative nature of the solution. In particular, the solution over the highly bending region converges to a linear polynomial as $m \to \infty$. In Section 5, we introduce the proposed preconditioner and prove its effectiveness by establishing a spectral bound for the preconditioned system. In Section 7, a strategy is presented on how to generalize the proposed preconditioner to cover high-contrast elliptic PDEs of order $2k$, $k>2$. In Section 6, the m- and h-robustness of the preconditioner are demonstrated by numerical experiments.

DOI: 10.1002/nla

2. THE UNDERLYING PDE AND THE LINEAR SYSTEM

We study the following high-contrast biharmonic equation for the clamped plate problem:

$$\begin{aligned} \nabla^2(\alpha\nabla^2 u) &= f \quad \text{in } \Omega\subset\mathbb{R}^2, \\ u=\partial_n u &= 0 \quad \text{on } \partial\Omega. \end{aligned} \tag{2}$$

We restrict the plate bending process to a *binary regime* (see Figure 1) in which the coefficient α is a piecewise constant function with the following values:

$$\alpha(x)=\begin{cases} m\gg 1, & x\in\Omega_{\mathrm{H}}, \\ 1, & x\in\Omega_{\mathrm{L}}. \end{cases} \tag{3}$$

It is quite common to idealize the discontinuous PDE coefficient α by a piecewise constant function [20, 21]. In the case of high-contrast diffusion equation, Aksoylu and Beyer [22] showed that the idealization of diffusivity by piecewise constant coefficients is meaningful by showing a continuous dependence of the solutions on the diffusivity; also see [23]. A similar justification can be extended to the high-contrast biharmonic plate equation.

2.1. Bilinear forms for the biharmonic equation

In the theory of elasticity, potential energy is defined by using *rotationally invariant* functions. For plates, the potential energy is given by [24, p. 30]:

$$J(v):=\frac{1}{2}\int_\Omega \alpha[\{\text{trace Hess}\}^2+2(\sigma-1)\det\text{Hess}]\,\mathrm{d}x-\int_\Omega fv\,\mathrm{d}x, \tag{4}$$

where Hess is the Hessian,

$$\text{Hess}=\begin{bmatrix} \partial_{11}v & \partial_{12}v \\ \partial_{21}v & \partial_{22}v \end{bmatrix}.$$

The bilinear form corresponding to energy minimization in (4) is given by

$$a(u,v):=\int_\Omega \alpha[\nabla^2 u\nabla^2 v+(1-\sigma)\{2\partial_{12}u\partial_{12}v-\partial_{11}u\partial_{22}v-\partial_{22}u\partial_{11}v\}]\,\mathrm{d}x, \tag{5}$$

where $0<\sigma<\frac{1}{2}$ is the Poisson ratio. Note that the straightforward bilinear form associated with (2) is obtained by using Green's formula:

$$\int_\Omega \nabla^2(\alpha\nabla^2 u)v\,\mathrm{d}x=\int_\Omega \alpha\nabla^2 u\nabla^2 v\,\mathrm{d}x+\int_{\partial\Omega}\alpha\partial_n\nabla^2 u v\,\mathrm{d}\gamma-\int_{\partial\Omega}\alpha\nabla^2 u\partial_n v\,\mathrm{d}\gamma. \tag{6}$$

We see that both (5) and (6) contain the so-called *canonical* bilinear form, $\tilde{a}(u,v)$, associated with the biharmonic equation (2):

$$\tilde{a}(u,v):=\int_\Omega \alpha\nabla^2 u\nabla^2 v\,\mathrm{d}x. \tag{7}$$

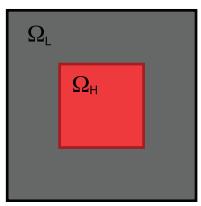

Figure 1. $\Omega=\overline{\Omega}_{\mathrm{H}}\cup\Omega_{\mathrm{L}}$ where Ω_{H} and Ω_{L} are highly and lowly bending regions, respectively.

DOI: 10.1002/nla

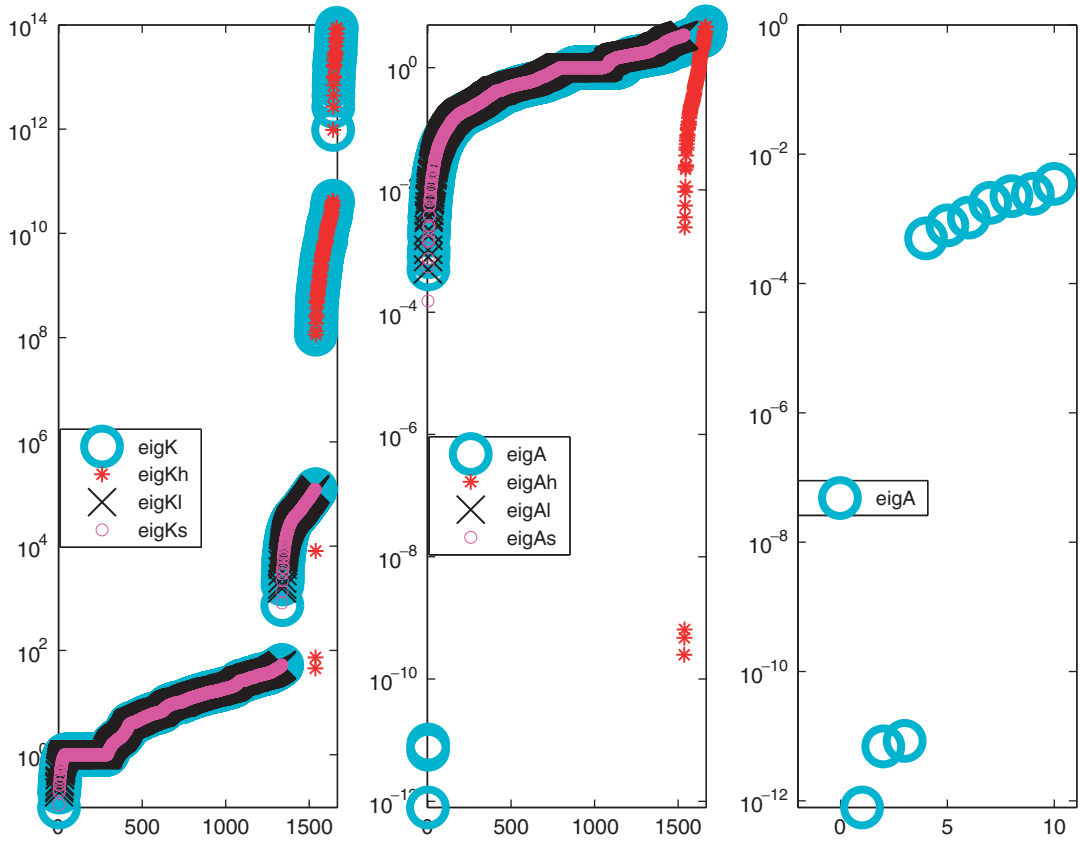

Figure 2. The HCT discretization of the biharmonic equation with $m = 10^9$. (Left) The spectrum of the stiffness matrix K. (Middle) Spectrum of the diagonally scaled stiffness matrix. (Right) The zoomed out version of the three smallest eigenvalue of diagonally scaled matrix. Notice the three small eigenvalues of order $\mathcal{O}(m^{-1})$ corresponding to the kernel of the Neumann matrix, span $\{\underline{1}_H, \underline{x}_H, \underline{y}_H\}$.

When $u, v \in H_0^2(\Omega)$, both bilinear forms $a(u, v)$ and $\tilde{a}(u, v)$ correspond to the strong formulation (2) due to second Green's formula and the zero contribution of the following term:

$$\int_\Omega (1-\sigma)\{2\partial_{12}u\partial_{12}v - \partial_{11}u\partial_{22}v - \partial_{22}u\partial_{11}v\}\,\mathrm{d}x. \tag{8}$$

2.2. *Effects of high-contrast on the spectrum*

Roughness of PDE coefficients causes loss of robustness of preconditioners. This is mainly due to clusters of eigenvalues with varying magnitude. Although diagonal scaling has no effect on the asymptotic behavior of the condition number, it leads to an improved clustering in the spectrum. The spectrum of the diagonally scaled stiffness matrix, A, is bounded from above and below except three eigenvalues in the case of a single isolated highly bending island. On the other hand, the spectrum of K contains eigenvalues approaching infinity with cardinality depending on the number of degrees of freedom (DOF) contained within the highly bending island. For the case of $m = 10^9$, we depict the spectra of K and A and their subblocks in Figure 2. Clustering provided by diagonal scaling can be advantageous for faster convergence of Krylov subspace solvers especially when deflation methods designed for small eigenvalues are used; for further discussion see [25].

Utilizing the matrix entry-based analysis by Graham and Hagger [26] for linear finite elements (FE), in [2], the authors extended the spectral analysis to cell-centered finite volume discretization and obtained an identical spectral result for A. Namely, the number of small eigenvalues of A depends on the number of isolated islands comprising the highly bending region. We observe a

DOI: 10.1002/nla

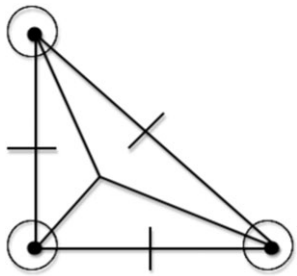

Figure 3. HCT element.

similar behavior for the biharmonic plate equation where the only difference is that for each island we observe three small eigenvalues rather than one. The three-dimensional kernel of the Neumann matrix is responsible for that difference; see Section 3. A similar matrix entry-based analysis can be applied to this problem, but this analysis is more involved for the Hsieh–Clough–Tocher (HCT) discretization than that for linear FE. Hence, we exclude it from the scope of this article.

3. DISCRETIZATION AND LRPS

We consider an H^2-conformal Galerkin finite element discretization with an HCT element. The HCT element is constructed by subdividing the triangle element into three subtriangles by connecting its vertices to its centroid. Then, a C^1 function consisting of piecewise cubic polynomials defined on each subtriangle is built. The function value and its first derivatives are specified on the vertices of the original triangle, and the normal derivative of the function is specified on the midpoint of each sides of the triangle; see Figure 3. HCT element is conforming but nonnested, and consists of 12 DOF. For a more detailed definition of the HCT element, see [27].

Let the linear system arising from the discretization be denoted by:

$$K(m)\, x = b. \tag{9}$$

Ω is decomposed with respect to magnitude of the coefficient value as

$$\Omega = \overline{\Omega}_{\mathrm{H}} \cup \Omega_{\mathrm{L}}, \tag{10}$$

where Ω_{H} and Ω_{L} denote the highly and lowly bending regions, respectively. DOF that lie on the interface, $\Gamma := \overline{\Omega}_{\mathrm{H}} \cap \overline{\Omega}_{\mathrm{L}}$, between the two regions are included in Ω_{H}. When m-dependence is explicitly stated and the discretization system (9) is decomposed with respect to (10), i.e. the magnitude of the coefficient values, we arrive at the following 2×2 block system:

$$\begin{bmatrix} K_{\mathrm{HH}}(m) & K_{\mathrm{HL}} \\ K_{\mathrm{LH}} & K_{\mathrm{LL}} \end{bmatrix} \begin{bmatrix} x_{\mathrm{H}} \\ x_{\mathrm{L}} \end{bmatrix} = \begin{bmatrix} b_{\mathrm{H}} \\ b_{\mathrm{L}} \end{bmatrix}. \tag{11}$$

There are important properties associated with the K_{HH} block in (11): It is the only block that has m-dependence, and furthermore, a matrix with a low-rank kernel can be extracted from it. Our preconditioner construction is based on LRPs from this extraction. Next, we explain how to extract the so-called *Neumann matrix* and why $a(u, v)$ is the suitable bilinear form for that purpose.

By rewriting (5) as the following:

$$a(u, v) = \int_{\Omega} \alpha[\sigma \nabla^2 u \nabla^2 v + (1-\sigma)\{\partial_{11} u \partial_{11} v + \partial_{22} u \partial_{22} v + 2\partial_{12} u \partial_{12} v\}]\, \mathrm{d}x, \tag{12}$$

DOI: 10.1002/nla

we see that

$$a(v,v) = \alpha\sigma\|\nabla^2 v\|^2_{L_2(\Omega)} + \alpha(1-\sigma)|v|^2_{H^2(\Omega)}$$
$$\geqslant \alpha(1-\sigma)|v|^2_{H^2(\Omega)}. \tag{13}$$

The inequality (13) has important implications. Namely, $a(v,v)$ is $V_{\mathscr{P}_1}(\Omega)$-coercive where $V_{\mathscr{P}_1}(\Omega) \subset H^2(\Omega)$ is a closed subspace such that $V_{\mathscr{P}_1}(\Omega) \cap \mathscr{P}_1 = \emptyset$ and $\mathscr{P}_1$ denotes the set of polynomials of degree at most 1. Furthermore, (13) immediately implies that $a(v,v)$ is $H^2_0(\Omega)$-coercive.

Let $\mathscr{T}^h$ be the triangulation of Ω and $V^h(\Omega)$ be the associated discrete space. Let $V^h(\overline{\Omega}_{\mathrm{H}})$ be the restriction of $V^h(\Omega)$ onto $\overline{\Omega}_{\mathrm{H}}$ based on the decomposition in (10). We define the *Neumann matrix* $\mathscr{N}_{\mathrm{HH}}$ as follows:

$$\langle \mathscr{N}_{\mathrm{HH}} \underline{\phi}^h_{\mathrm{H}}, \underline{\psi}^h_{\mathrm{H}} \rangle := a(\phi^h_{\mathrm{H}}, \psi^h_{\mathrm{H}}),$$

where $\phi^h_{\mathrm{H}}, \psi^h_{\mathrm{H}} \in V^h(\overline{\Omega}_{\mathrm{H}})$ are the basis functions whose values of DOF are denoted by $\underline{\phi}^h_{\mathrm{H}}$ and $\underline{\psi}^h_{\mathrm{H}}$, respectively. Since $a(\cdot,\cdot)$ is $V_{\mathscr{P}_1}(\Omega)$-coercive, this implies by (13) that

$$\ker \mathscr{N}_{\mathrm{HH}} = \mathscr{P}^h_1|_{\overline{\Omega}_{\mathrm{H}}} = \mathrm{span}\{\underline{1}_{\mathrm{H}}, \underline{x}_{\mathrm{H}}, \underline{y}_{\mathrm{H}}\}. \tag{14}$$

Hence, with m defined in (3), K_{HH} in (11) has the following decomposition:

$$K_{\mathrm{HH}}(m) = m\mathscr{N}_{\mathrm{HH}} + R, \tag{15}$$

where R is the coupling matrix corresponding to DOF on the interface Γ.

Now, we are in a position to reveal the resulting main numerical linear algebra implication. As $m \to \infty$, the limiting Schur complement S_∞ in (1) becomes a rank-3 perturbation of K_{LL}. This result relies on the fact that the inverse of the limiting K_{HH} is of rank-3; see (17). This is due to the fact that $\mathscr{N}_{\mathrm{HH}}$ has a rank-3 kernel whose (normalized) discretization is given by:

$$\mathrm{e}_{\mathrm{H}} := [\underline{1}_{\mathrm{H}}, \underline{x}_{\mathrm{H}}, \underline{y}_{\mathrm{H}}]. \tag{16}$$

4. MAIN SPA RESULTS

Lemma 4.1
The asymptotic behavior of the submatrices in (30) is given as follows:

$$K_{\mathrm{HH}}(m)^{-1} = \mathrm{e}_{\mathrm{H}}\eta^{-1}\mathrm{e}^{\mathrm{t}}_{\mathrm{H}} + \mathscr{O}(m^{-1}), \tag{17}$$

$$S(m) = K_{\mathrm{LL}} - (K_{\mathrm{LL}}\mathrm{e}_{\mathrm{H}})\eta^{-1}(\mathrm{e}^{\mathrm{t}}_{\mathrm{H}}K_{\mathrm{LL}}) + \mathscr{O}(m^{-1}), \tag{18}$$

$$K_{\mathrm{LH}}K_{\mathrm{HH}}(m)^{-1} = (K_{\mathrm{LL}}\,\mathrm{e}_{\mathrm{H}})\eta^{-1}\,\mathrm{e}^{\mathrm{t}}_{\mathrm{H}} + \mathscr{O}(m^{-1}), \tag{19}$$

where

$$\eta := \mathrm{e}^{\mathrm{t}}_{\mathrm{H}}K_{\mathrm{HH}}\mathrm{e}_{\mathrm{H}}. \tag{20}$$

Proof
Since $\mathscr{N}_{\mathrm{HH}}$ is symmetric positive semidefinite, using (14) we have the following spectral decomposition where n_{H} denotes the cardinality of DOF in $\overline{\Omega}_{\mathrm{H}}$:

$$Z^{\mathrm{t}}\mathscr{N}_{\mathrm{HH}}Z = \mathrm{diag}(\lambda_1, \ldots, \lambda_{n_{\mathrm{H}}-3}, 0, 0, 0), \tag{21}$$

where $\{\lambda_i : i = 1, \ldots, n_{\mathrm{H}}\}$ is a nonincreasing sequence of eigenvalues of $\mathscr{N}_{\mathrm{HH}}$ and Z is orthogonal. Since, the eigenvectors corresponding to the zero eigenvalues are discretizations of the polynomials

DOI: 10.1002/nla

1, x, and y, we can write $Z=[\tilde{Z}|\mathrm{e}_{\mathrm{H}}]$ where e_{H} is defined in (16). Using (15), we have:

$$Z^{\mathrm{t}}K_{\mathrm{HH}}(m)Z = \begin{bmatrix} m\,\mathrm{diag}(\lambda_1,\ldots,\lambda_{n_{\mathrm{H}}-3})+\tilde{Z}^{\mathrm{t}}R\tilde{Z} & \tilde{Z}^{\mathrm{t}}R\mathrm{e}_{\mathrm{H}} \\ \mathrm{e}_{\mathrm{H}}^{\mathrm{t}}R\tilde{Z} & \mathrm{e}_{\mathrm{H}}^{\mathrm{t}}R\mathrm{e}_{\mathrm{H}} \end{bmatrix} =: \begin{bmatrix} \tilde{\Lambda}(m) & \tilde{\delta} \\ \tilde{\delta}^{\mathrm{t}} & \eta \end{bmatrix}. \tag{22}$$

To find the limiting form of $K_{\mathrm{HH}}(m)^{-1}$ note that

$$\begin{aligned}\tilde{\Lambda}(m) &= m\,\mathrm{diag}(\lambda_1,\ldots,\lambda_{n_{\mathrm{H}}-3})+\tilde{Z}^{\mathrm{t}}R\tilde{Z} \\ &= m\,\mathrm{diag}(\lambda_1,\ldots,\lambda_{n_{\mathrm{H}}-3})(\tilde{I}+m^{-1}\,\mathrm{diag}(\lambda_1^{-1},\ldots,\lambda_{n_{\mathrm{H}}-3}^{-1})\tilde{Z}^{\mathrm{t}}R\tilde{Z}).\end{aligned}$$

Then,

$$\|\tilde{\Lambda}(m)^{-1}\|_2 \leqslant \frac{m^{-1}\max_{i\leqslant n_{\mathrm{H}}-3}\lambda_i^{-1}}{1-m^{-1}\max_{i\leqslant n_{\mathrm{H}}-3}\lambda_i^{-1}\|\tilde{Z}^{\mathrm{t}}R\tilde{Z}\|_2}.$$

For sufficiently large m, we can conclude the following:

$$\tilde{\Lambda}(m)^{-1}=\mathcal{O}(m^{-1}). \tag{23}$$

We proceed with the following inversion:

$$\begin{bmatrix} \tilde{\Lambda}(m) & \tilde{\delta} \\ \tilde{\delta}^{\mathrm{t}} & \eta \end{bmatrix}^{-1} = U(m)V(m)U(m)^{\mathrm{t}},$$

where

$$U(m) := \begin{bmatrix} \tilde{I} & -\tilde{\Lambda}(m)^{-1}\tilde{\delta} \\ 0^{\mathrm{t}} & 1 \end{bmatrix},$$

$$V(m) := \begin{bmatrix} \tilde{\Lambda}(m)^{-1} & 0 \\ 0^{\mathrm{t}} & (\eta-\tilde{\delta}^{\mathrm{t}}\tilde{\Lambda}(m)^{-1}\tilde{\delta})^{-1} \end{bmatrix}.$$

Then, (23) implies that

$$U(m) = I+\mathcal{O}(m^{-1}),$$

$$V(m) = \begin{bmatrix} O & 0 \\ 0^{\mathrm{t}} & \eta^{-1} \end{bmatrix}+\mathcal{O}(m^{-1}).$$

Combining the above results, we arrive at

$$\begin{bmatrix} \tilde{\Lambda}(m) & \tilde{\delta} \\ \tilde{\delta}^{\mathrm{t}} & \eta \end{bmatrix}^{-1} = \begin{bmatrix} O & 0 \\ 0^{\mathrm{t}} & \eta^{-1} \end{bmatrix}+\mathcal{O}(m^{-1}),$$

and, by (22), we have

$$\begin{aligned}K_{\mathrm{HH}}(m)^{-1} &= Z\begin{bmatrix} O & 0 \\ 0^{\mathrm{t}} & \eta^{-1} \end{bmatrix}Z^{\mathrm{t}}+\mathcal{O}(m^{-1}) \\ &=: \mathrm{e}_{\mathrm{H}}\eta^{-1}\mathrm{e}_{\mathrm{H}}^{\mathrm{t}}+\mathcal{O}(m^{-1}),\end{aligned} \tag{24}$$

which proves (17) of the Lemma.

Parts (18) and (19) follow from simple substitution and using (31). □

DOI: 10.1002/nla

Remark 4.1
If we further decompose DOF associated with $\overline{\Omega}_{\mathrm{H}}$ into a set of interior DOF associated with index I and interface DOF with index Γ, we obtain the following block representation of K_{HH}:

$$K_{\mathrm{HH}}(m)=\begin{bmatrix} K_{II}(m) & K_{I\Gamma}(m) \\ K_{\Gamma I}(m) & K_{\Gamma\Gamma}(m) \end{bmatrix}. \tag{25}$$

The entries in the block $K_{\Gamma\Gamma}(m)$ are assembled from contributions both from finite elements in Ω_{H} and Ω_{L}, i.e. $K_{\Gamma\Gamma}(m)=A^{(H)}_{\Gamma\Gamma}(m)+A^{(L)}_{\Gamma\Gamma}$.

We further write e_{H} in block form; $\mathrm{e}_{\mathrm{H}}=(\mathrm{e}^{\mathrm{t}}_I, \mathrm{e}^{\mathrm{t}}_\Gamma)^{\mathrm{t}}$. Finally, we note that the off-diagonal blocks have the decomposition:

$$K_{\mathrm{LH}}=[0 \;\; K_{L\Gamma}]=K^{\mathrm{t}}_{\mathrm{HL}}. \tag{26}$$

Therefore, the results of Lemma 4.1 can be rewritten as follows:

$$\begin{aligned} K_{\mathrm{HH}}(m)^{-1} &= \mathrm{e}_{\mathrm{H}}(\mathrm{e}^{\mathrm{t}}_\Gamma K^{(L)}_{\Gamma\Gamma}\mathrm{e}_\Gamma)^{-1}\mathrm{e}^{\mathrm{t}}_{\mathrm{H}}+\mathcal{O}(m^{-1}), \\ S(m) &= K_{\mathrm{LL}}-(K_{L\Gamma}\mathrm{e}_\Gamma)(\mathrm{e}^{\mathrm{t}}_\Gamma K^{(L)}_{\Gamma\Gamma}\mathrm{e}_\Gamma)^{-1}(\mathrm{e}^{\mathrm{t}}_\Gamma K_{\Gamma L})+\mathcal{O}(m^{-1}), \\ K_{\mathrm{LH}}K_{\mathrm{HH}}(m)^{-1} &= (K_{L\Gamma}\mathrm{e}_\Gamma)(\mathrm{e}^{\mathrm{t}}_\Gamma K^{(L)}_{\Gamma\Gamma}\mathrm{e}_\Gamma)^{-1}\mathrm{e}^{\mathrm{t}}_{\mathrm{H}}+\mathcal{O}(m^{-1}). \end{aligned}$$

We will use the following limit values of the block matrices (in Lemma 4.1) in the definition of the preconditioner in (32):

$$K^{\infty}_{\mathrm{HH}} := \mathrm{e}_{\mathrm{H}}\eta^{-1}\mathrm{e}^{\mathrm{t}}_{\mathrm{H}}, \tag{27}$$

$$S_\infty := K_{\mathrm{LL}}-K_{\mathrm{LH}}K^{\infty}_{\mathrm{HH}}K_{\mathrm{HL}}. \tag{28}$$

4.1. Qualitative nature of the solution

We advocate the usage of SPA because it is a very effective tool in gaining qualitative insight about the asymptotic behavior of the solution of the underlying PDE. Through SPA, in Lemma 4.1, we were able to fully reveal the asymptotic behavior of the submatrices of K in (30). This information leads to a characterization of the limit of the underlying discretized inverse operator. We now prove that *the solution over the highly bending island converges to a linear polynomial*. In other words, $x^{\infty}_{\mathrm{H}}\in \operatorname{span}\mathrm{e}_{\mathrm{H}}$. This is probably the most fundamental qualitative feature of the solution of the high-contrast biharmonic plate equation.

Lemma 4.2
Let e_{H} be as in (16). Then,

$$x_{\mathrm{H}}(m)=\mathrm{e}_{\mathrm{H}}c_{\mathrm{H}}+\mathcal{O}(m^{-1}), \tag{29}$$

where c_{H} is a 3×1 vector determined by the solution in the lowly bending region.

Proof
We prove the result by providing an explicit quantification of the limiting process based on Lemma 4.1:

$$\begin{aligned} x_{\mathrm{L}}(m) &= S^{-1}(m)\{b_{\mathrm{L}}-K_{\mathrm{LH}}K^{-1}_{\mathrm{HH}}(m)b_{\mathrm{H}}\} \\ &= S^{-1}_\infty\{b_{\mathrm{L}}-K_{\mathrm{LH}}(\mathrm{e}_{\mathrm{H}}\eta^{-1}\mathrm{e}^{\mathrm{t}}_{\mathrm{H}})b_{\mathrm{H}}\}+\mathcal{O}(m^{-1}) \\ &=: x^{\infty}_{\mathrm{L}}+\mathcal{O}(m^{-1}), \end{aligned}$$

DOI: 10.1002/nla

$$\begin{aligned} x_{\mathrm{H}}(m) &= K_{\mathrm{HH}}^{-1}(m)\{b_{\mathrm{H}} - K_{\mathrm{HL}}x_{\mathrm{L}}(m)\} \\ &= \mathrm{e}_{\mathrm{H}}\eta^{-1}\mathrm{e}_{\mathrm{H}}^{\mathrm{t}}\{b_{\mathrm{H}} - K_{\mathrm{HL}}x_{\mathrm{L}}^{\infty}\} + \mathcal{O}(m^{-1}) \\ &=: \mathrm{e}_{\mathrm{H}}c_{\mathrm{H}} + \mathcal{O}(m^{-1}). \end{aligned}$$ □

5. CONSTRUCTION OF THE PRECONDITIONER

The exact inverse of K can be written as:

$$K^{-1} = \begin{bmatrix} I_{\mathrm{HH}} & -K_{\mathrm{HH}}^{-1}K_{\mathrm{HL}} \\ 0 & I_{\mathrm{LL}} \end{bmatrix} \begin{bmatrix} K_{\mathrm{HH}}^{-1} & 0 \\ 0 & S^{-1} \end{bmatrix} \begin{bmatrix} I_{\mathrm{HH}} & 0 \\ -K_{\mathrm{LH}}K_{\mathrm{HH}}^{-1} & I_{\mathrm{LL}} \end{bmatrix}, \tag{30}$$

where I_{HH} and I_{LL} denote the identity matrices of the appropriate dimension and the Schur complement S is explicitly given by:

$$S(m) = K_{\mathrm{LL}} - K_{\mathrm{LH}}K_{\mathrm{HH}}^{-1}(m)K_{\mathrm{HL}}. \tag{31}$$

Let the limit in (17) be denoted by $K_{\mathrm{HH}}^{\infty} := \mathrm{e}_{\mathrm{H}}\eta^{-1}\mathrm{e}_{\mathrm{H}}^{\mathrm{t}}$. Based on the above perturbation analysis, our proposed preconditioner is defined as follows:

$$B_{\mathrm{AGKS}}(m) := \begin{bmatrix} I_{\mathrm{HH}} & -K_{\mathrm{HH}}^{\infty}K_{\mathrm{HL}} \\ 0 & I_{\mathrm{LL}} \end{bmatrix} \begin{bmatrix} K_{\mathrm{HH}}(m)^{-1} & 0 \\ 0 & S_{\infty}^{-1} \end{bmatrix} \begin{bmatrix} I_{\mathrm{HH}} & 0 \\ -K_{\mathrm{LH}}K_{\mathrm{HH}}^{\infty} & I_{\mathrm{LL}} \end{bmatrix}, \tag{32}$$

where K_{HH}^{∞} and S_{∞} are defined in (27) and (28), respectively.

We need the following auxiliary result to be used in the proof of Theorem 5.1, which characterizes the spectral behavior of the preconditioned system.

Lemma 5.1
The following statement holds for $K_{\mathrm{HH}}^{-1/2}$:

$$K_{\mathrm{HH}}^{-1/2} = \mathrm{e}_{\mathrm{H}}\eta^{-1/2}\mathrm{e}_{\mathrm{H}}^{\mathrm{t}} + \mathcal{O}(m^{-1/2}), \tag{33}$$

where η is the 3×3 SPD matrix independent of m defined in (20).

Proof
We start by writing down the spectral decomposition of $K_{\mathrm{HH}}(m)$

$$Q(m)^{\mathrm{t}}K_{\mathrm{HH}}(m)Q(m) = \mathrm{diag}(\mu_1(m), \ldots, \mu_{n_{\mathrm{H}}-3}(m), \mu_{n_{\mathrm{H}}-2}(m), \mu_{n_{\mathrm{H}}-1}(m), \mu_{n_{\mathrm{H}}}(m)),$$

where $\{\mu_i(m) : i = 1, \ldots, n_{\mathrm{H}}\}$ denotes a nonincreasing ordering of the eigenvalues of $K_{\mathrm{HH}}(m)$. Since $K_{\mathrm{HH}}(m)$ is SPD, we have $\mu_i(m) > 0$ for all $i \leqslant n_{\mathrm{H}}$. We use the main fact that eigenvalues and eigenvectors of a symmetric matrix are Lipschitz continuous functions of the matrix entries [28, 29].

By (21) and (24) in Lemma 4.1, we give the following spectral decomposition:

$$K_{\mathrm{HH}}^{-1}(m) = z_1 0 z_1^{\mathrm{t}} + \cdots + z_{n_{\mathrm{H}}-3} 0 z_{n_{\mathrm{H}}-3}^{\mathrm{t}} + \mathrm{e}_{\mathrm{H}}\eta^{-1}\mathrm{e}_{\mathrm{H}}^{\mathrm{t}} + \mathcal{O}(m^{-1}). \tag{34}$$

Note that η in (22) is a 3×3 symmetric, and hence, diagonalizable matrix. We proceed toward a fully diagonalized form of the limiting $K_{\mathrm{HH}}^{-1}(m)$. For that, we use the diagonalization of η^{-1}:

$$\eta^{-1} = \hat{z}_{H_1}\mu_{H_1}^{-1}\hat{z}_{H_1}^{\mathrm{t}} + \hat{z}_{H_x}\mu_{H_x}^{-1}\hat{z}_{H_x}^{\mathrm{t}} + \hat{z}_{H_y}\mu_{H_y}^{-1}\hat{z}_{H_y}^{\mathrm{t}}.$$

Therefore, we have the following expression for the last term in (34):

$$\mathrm{e}_{\mathrm{H}}\eta^{-1}\mathrm{e}_{\mathrm{H}}^{\mathrm{t}} = [z_{H_1} \;\; z_{H_x} \;\; z_{H_y}]\mathrm{diag}(\mu_{H_1}^{-1}, \mu_{H_x}^{-1}, \mu_{H_y}^{-1})[z_{H_1} \;\; z_{H_x} \;\; z_{H_y}]^{\mathrm{t}}, \tag{35}$$

DOI: 10.1002/nla

where

$$[z_{H_1}\ \ z_{H_x}\ \ z_{H_y}] := [\mathrm{e}_{H_1}\ \ \mathrm{e}_{H_x}\ \ \mathrm{e}_{H_y}][\hat{z}_{H_1}\ \ \hat{z}_{H_x}\ \ \hat{z}_{H_y}],$$
$$[\mathrm{e}_{H_1}, \mathrm{e}_{H_x}, \mathrm{e}_{H_y}] := \mathrm{e}_{\mathrm{H}}.$$

Now by substituting (35) in (34), we have the following spectral decomposition that corresponds to the fully diagonalized version:

$$\begin{aligned} K_{\mathrm{HH}}^{-1}(m) &= z_1 0 z_1^{\mathrm{t}} + \cdots + z_{n_{\mathrm{H}}-3} 0 z_{n_{\mathrm{H}}-3}^{\mathrm{t}} + z_{H_1}\mu_{H_1} z_{H_1}^{\mathrm{t}} + z_{H_x}\mu_{H_x} z_{H_x}^{\mathrm{t}} + z_{H_y}\mu_{H_y} z_{H_y}^{\mathrm{t}} + \mathcal{O}(m^{-1}) \\ &=: Z_\infty \mathrm{diag}(0, \ldots, 0, \mu_{H_1}^{-1}, \mu_{H_x}^{-1}, \mu_{H_y}^{-1}) Z_\infty^{\mathrm{t}} + \mathcal{O}(m^{-1}). \end{aligned} \tag{36}$$

The expression in (36) also implies the convergence of the eigenvectors of $K_{\mathrm{HH}}(m)$:

$$Q(m) = Z_\infty + \mathcal{O}(m^{-1}). \tag{37}$$

Note that Z_∞ differs from Z in (21) only in the last three columns due to diagonalization of η.

From (36), we obtain a characterization of the largest three eigenvalues of $K_{\mathrm{HH}}(m)^{-1}$:

$$\mu_{n_{\mathrm{H}}-2}(m)^{-1} = \mu_{H_1}^{-1} + \mathcal{O}(m^{-1}), \tag{38a}$$

$$\mu_{n_{\mathrm{H}}-1}(m)^{-1} = \mu_{H_x}^{-1} + \mathcal{O}(m^{-1}), \tag{38b}$$

$$\mu_{n_{\mathrm{H}}}(m)^{-1} = \mu_{H_y}^{-1} + \mathcal{O}(m^{-1}). \tag{38c}$$

Using (36) and (38), we arrive at the following:

$$\begin{aligned} &\mathrm{diag}(\mu_1(m)^{-1/2}, \ldots, \mu_{n_{\mathrm{H}}-3}(m)^{-1/2}, \mu_{n_{\mathrm{H}}-2}(m)^{-1/2}, \mu_{n_{\mathrm{H}}-1}(m)^{-1/2}, \mu_{n_{\mathrm{H}}}(m)^{-1/2}) \\ &= \mathrm{diag}(0, \ldots, 0, \mu_{H_1}^{-1/2}, \mu_{H_x}^{-1/2}, \mu_{H_y}^{-1/2}) + \mathcal{O}(m^{-1/2}). \end{aligned} \tag{39}$$

By using (39) and (37), we arrive at the desired result:

$$\begin{aligned} K_{\mathrm{HH}}(m)^{-1/2} &= Q(m)\,\mathrm{diag}(\mu_1(m)^{-1/2}, \ldots, \mu_{n_{\mathrm{H}}}(m)^{-1/2}) Q(m)^{\mathrm{t}} \\ &= Z_\infty \mathrm{diag}(0, \ldots, 0, \mu_{H_1}^{-1/2}, \mu_{H_x}^{-1/2}, \mu_{H_y}^{-1/2}) Z_\infty^{\mathrm{t}} + \mathcal{O}(m^{-1/2}) \\ &= [z_{H_1}\ \ z_{H_x}\ \ z_{H_y}]\,\mathrm{diag}(\mu_{H_1}^{-1/2}, \mu_{H_x}^{-1/2}, \mu_{H_y}^{-1/2})[z_{H_1}\ \ z_{H_x}\ \ z_{H_y}]^{\mathrm{t}} + \mathcal{O}(m^{-1/2}) \\ &= \mathrm{e}_{\mathrm{H}} \eta^{-1/2} \mathrm{e}_{\mathrm{H}}^{\mathrm{t}} + \mathcal{O}(m^{-1/2}). \end{aligned}$$

□

The following theorem shows that B_{AGKS} is an effective preconditioner for $m \gg 1$.

Theorem 5.1
For sufficiently large m, we have

$$\sigma(B_{\mathrm{AGKS}}(m) K(m)) \subset [1 - cm^{-1/2}, 1 + cm^{-1/2}]$$

for some constant c independent of m, and therefore

$$\kappa(B_{\mathrm{AGKS}}(m)\ K(m)) = 1 + \mathcal{O}(\mathrm{m}^{-1/2}).$$

Proof
Let us factorize the preconditioner as $B_{\mathrm{AGKS}} = L^{\mathrm{t}} L$ with

$$L := \begin{bmatrix} K_{\mathrm{HH}}(m)^{-1/2} & 0 \\ -S_\infty^{-1/2} P_{\mathrm{LH}}^\infty & S_\infty^{-1/2} \end{bmatrix},$$

DOI: 10.1002/nla

where the limiting Schur complement $S(m)$ and $K_{\mathrm{LH}}K_{\mathrm{HH}}^{-1}$ is denoted by S_∞ and P_{LH}^{∞}, respectively. We can easily show that

$$\sigma(B_{\mathrm{AGKS}}K)=\sigma(LKL^{\mathrm{t}})=\sigma(I+E). \tag{40}$$

Note that

$$P_{\mathrm{LH}}^{\infty}K_{\mathrm{HH}}P_{\mathrm{LH}}^{\infty^{\mathrm{t}}}-P_{\mathrm{LH}}^{\infty}K_{\mathrm{HL}}=K_{\mathrm{LH}}(\mathrm{e}_{\mathrm{H}}\eta^{-1}\,\mathrm{e}_{\mathrm{H}}^{t}K_{\mathrm{HH}}\mathrm{e}_{\mathrm{H}}\eta^{-1}\,\mathrm{e}_{\mathrm{H}}^{\mathrm{t}}-\mathrm{e}_{\mathrm{H}}\eta^{-1}\,\mathrm{e}_{\mathrm{H}}^{\mathrm{t}})K_{\mathrm{HL}}=0. \tag{41}$$

We give a step of the operation leading to (40). Using (41), the (2,2)th block entry of the LKL^{t} reads:

$$S_\infty^{-1/2}[P_{\mathrm{LH}}^{\infty}K_{\mathrm{HH}}P_{\mathrm{LH}}^{\infty^{\mathrm{t}}}-P_{\mathrm{LH}}^{\infty}K_{\mathrm{HL}}-K_{\mathrm{LH}}P_{\mathrm{LH}}^{\infty^{\mathrm{t}}}+K_{\mathrm{LL}}]S_\infty^{-1/2}=I.$$

The other entries of LKL^{t} can be computed in a similar way.

Using (33), we have

$$E_{\mathrm{LH}}=S_\infty^{-1/2}K_{\mathrm{LH}}(I_{\mathrm{HH}}-\mathrm{e}_{\mathrm{H}}\eta^{-1}\,\mathrm{e}_{\mathrm{H}}^{\mathrm{t}}K_{\mathrm{HH}})\mathrm{e}_{\mathrm{H}}\eta^{-1/2}\,\mathrm{e}_{\mathrm{H}}^{\mathrm{t}}+\mathcal{O}(m^{-1/2})=\mathcal{O}(m^{-1/2}).$$

Hence $\rho(E)$, the spectral radius of E, is $\mathcal{O}(m^{-1/2})$, which together with (40) completes the proof. □

6. NUMERICAL EXPERIMENTS

The goal of the numerical experiments is to compare the performance of the two preconditioners: AGKS and MG. The domain is a unit square whose coarsest-level triangulation consists of 32 triangles. We consider the case of a single highly bending island located at the region $[\frac{1}{4},\frac{2}{4}]\times[\frac{1}{4},\frac{2}{4}]$ consisting of two coarsest-level triangles. For an extension, we also consider the cases of the L-shaped island and the two disconnected islands. The implementation of HCT discretization is based on Pozrikidis' software provided in [16]. For these experiments, the problem sizes are 131, 451, 1,667, 6,403 for levels 1, 2, 3, and 4.

We denote the norm of the relative residual at iteration i by $\mathrm{rr}^{(i)}$:

$$\mathrm{rr}^{(i)}:=\frac{\|r^{(i)}\|_2}{\|r^{(0)}\|_2},$$

where $r^{(i)}$ denotes the residual at iteration i with a stopping criterion of $\mathrm{rr}^{(i)}\leqslant 10^{-7}$. In Tables I–V, the preconditioned conjugate gradient iteration count and the average reduction factor are reported for combinations of preconditioner, smoother types, and the number of smoothing iterations. The average reduction factor of the residual is defined as:

$$(\mathrm{rr}^{(i)})^{1/i}.$$

We enforce an iteration bound of 60. If the method seems to converge slightly beyond this bound, we denote it by 60^{+}, whereas stalling is denoted by ∞.

We use the Galerkin variational approach to construct the coarser-level algebraic systems. The multigrid preconditioner MG is derived from the implementation by Aksoylu *et al.* [30]. We employ a $V(s,s)$-cycle, $s=1$, 5, 10, with point symmetric Gauss–Seidel (sGS) and point Gauss–Seidel (GS) smoothers. A direct solver is used for the coarsest level.

DOI: 10.1002/nla

Table I. Single Island Case: AGKS+HCT+sGS+smooth number 1-5-10.

$N\backslash m$	10^0	10^1	10^2	10^3	10^4	10^5	10^7	10^9	10^{10}
Smooth number=1									
131	**24**, 0.485	**20**, 0.447	**18**, 0.407	**17**, 0.371	**17**, 0.381	**16**, 0.337	**18**, 0.371	**16**, 0.362	**17**, 0.384
451	**52**, 0.730	**38**, 0.650	**21**, 0.452	**13**, 0.286	**12**, 0.249	**12**, 0.256	**13**, 0.279	**12**, 0.253	**11**, 0.213
1667	**60**$^+$, 0.857	**60**$^+$,0.768	**33**, 0.610	**20**, 0.426	**18**, 0.401	**19**, 0.410	**21**, 0.447	**19**, 0.420	**19**, 0.417
6403	∞, 0.972	**60**$^+$, 0.930	**60**$^+$, 0.839	**45**, 0.692	**37**, 0.637	**36**, 0.636	**36**, 0.638	**36**, 0.635	**39**, 0.661
Smooth number=5									
131	**24**, 0.485	**20**, 0.447	**18**, 0.407	**17**, 0.371	**17**, 0.381	**16**, 0.337	**18**, 0.371	**16**, 0.362	**17**, 0.384
451	**40**, 0.664	**28**, 0.547	**15**, 0.330	**8**, 0.131	**6**, 0.054	**6**, 0.023	**4**, 0.014	**4**, 0.016	**4**, 0.012
1667	**60**$^+$, 0.786	**48**, 0.706	**24**, 0.490	**12**, 0.258	**8**, 0.091	**6**, 0.058	**5**, 0.035	**5**, 0.026	**5**, 0.024
6403	**60**$^+$, 0.947	**60**$^+$, 0.862	**43**, 0.682	**21**, 0.427	**12**, 0.223	**8**, 0.091	**6**, 0.051	**6**, 0.052	**6**, 0.062
Smooth number=10									
131	**24**, 0.485	**20**, 0.447	**18**, 0.407	**17**, 0.371	**17**, 0.381	**16**, 0.337	**18**, 0.371	**16**, 0.362	**17**, 0.384
451	**37**, 0.634	**26**, 0.528	**15**, 0.330	**8**, 0.131	**6**, 0.050	**6**, 0.017	**4**, 0.010	**3**, 0.004	**3**, 0.003
1667	**60**$^+$, 0.785	**43**, 0.680	**20**, 0.442	**12**, 0.213	**8**, 0.080	**6**, 0.030	**4**, 0.004	**4**, 0.002	**4**, 0.008
6403	**60**$^+$, 0.943	**60**$^+$, 0.861	**38**, 0.653	**20**, 0.410	**10**, 0.177	**8**, 0.090	**5**, 0.028	**5**, 0.015	**5**, 0.023

Bold characters indicate iteration counts and the number of DOF in the linear system.

Table II. Single Island Case: MG+HCT+sGS+smooth number 1-5-10.

$N\backslash m$	10^0	10^1	10^2	10^4	10^5	10^6	10^7	10^8	10^9
Smooth number=1									
131	**60**$^+$, 0.885	**60**$^+$, 0.898	**60**$^+$, 0.932	∞, 0.988	∞, 0.997	∞, 1.075	∞, 1.089	∞, 1.065	∞, 1.137
451	∞, 0.963	∞, 0.987	∞ 1.014	∞, 1.050	∞, 1.086	∞, 1.106	∞, 1.172	∞, 1.081	∞, 1.091
1667	∞, 0.985	∞, 1.015	∞, 1.044	∞, 1.062	∞, 1.122	∞, 1.109	∞, 1.142	∞, 1.170	∞, 1.124
6403	∞, 1.025	∞, 1.040	∞, 1.057	∞, 1.125	∞, 1.145	∞, 1.130	∞, 1.171	∞, 1.112	∞, 1.187
Smooth number=5									
131	**60**$^+$, 0.885	**60**$^+$, 0.898	**60**$^+$, 0.932	∞, 0.988	∞, 0.997	∞, 1.075	∞, 1.089	∞, 1.065	∞, 1.137
451	**60**$^+$, 0.761	**60**$^+$, 0.829	**60**$^+$, 0.920	∞, 1.070	∞, 1.084	∞, 1.120	∞, 1.174	∞, 1.118	∞, 1.166
1667	**60**$^+$, 0.854	**60**$^+$, 0.923	∞, 0.999	∞, 1.038	∞, 1.0037	∞, 1.0085	∞, 1.134	∞, 1.154	∞, 1.208
6403	**60**$^+$, 0.931	∞, 0.979	∞, 0.998	∞,1.012	∞, 1.023	∞, 1.058	∞, 1.041	∞, 1.063	∞, 1.099
Smooth number=10									
131	**60**$^+$, 0.885	**60**$^+$, 0.898	**60**$^+$, 0.932	∞, 0.988	∞, 0.997	∞, 1.075	∞, 1.089	∞, 1.065	∞, 1.137
451	**48**, 0.660	**53**, 0.701	**60**$^+$, 0.825	∞, 0.955	∞, 1.032	∞, 1.115	∞, 1.179	∞, 1.200	∞, 1.196
1667	**40**, 0.624	**49**, 0.680	**60**$^+$, 0.797	∞, 1.001	∞, 1.088	∞, 1.035	∞, 1.064	∞, 1.052	∞, 1.095
6403	**60**$^+$, 0.890	**60**$^+$, 0.929	∞, 0.972	∞, 1.049	∞, 1.017	∞, 1.052	∞, 1.051	∞, 1.134	∞, 1.170

Bold characters indicate iteration counts and the number of DOF in the linear system.

Table III. L-shaped Island Case: AGKS+HCT+sGS+smooth number 1-5-10.

$N\backslash m$	10^0	10^1	10^2	10^3	10^4	10^5	10^7	10^9	10^{10}
Smooth number=1									
131	**23**, 0.515	**20**, 0.4878	**15**, 0.378	**12**, 0.310	**10**, 0.247	**9**, 0.148	**9**, 0.168	∞, 1.055	∞, 1.132
451	**60**$^+$, 0.801	**49**, 0.745	**35**, 0.657	**25**, 0.544	**21**, 0.491	**21**, 0.421	**22**, 0.529	**25**, 0.570	**25**, 0.573
1667	∞, 0.961	**60**$^+$,0.893	**60**$^+$, 0.818	**50**, 0.735	**47**, 0.730	**49**, 0.742	**37**, 0.727	**40**, 0.830	**47**, 0.819
Smooth number=5									
131	**23**, 0.515	**20**, 0.4878	**15**, 0.378	**12**, 0.310	**10**, 0.247	**9**, 0.148	**9**, 0.168	∞, 1.055	∞, 1.132
451	**54**, 0.770	**44**, 0.709	**27**, 0.579	**17**, 0.443	**13**, 0.321	**11**, 0.254	**9**, 0.112	**9**, 0.149	**9**, 0.233
1667	∞, 0.964	**60**$^+$, 0.893	**44**, 0.730	**25**, 0.559	**18**, 0.406	**14**, 0.367	**11**, 0.289	**10**, 0.292	**19**, 0.379
Smooth number=10									
131	**23**, 0.515	**20**, 0.4878	**15**, 0.378	**12**, 0.310	**10**, 0.247	**9**, 0.148	**9**, 0.168	∞, 1.055	∞, 1.132
451	**54**, 0.771	**44**, 0.709	**27**, 0.571	**18**, 0.441	**14**, 0.313	**11**, 0.244	**9**, 0.157	**9**, 0.147	**9**, 0.268
1667	∞, 0.964	**60**$^+$, 0.893	**44**, 0.708	**25**, 0.564	**17**, 0.400	**13**, 0.280	**11**, 0.250	**10**,0.278	**18**, 0.412

Bold characters indicate iteration counts and the number of DOF in the linear system.

DOI: 10.1002/nla

Table IV. L-shaped Island Case: MG+HCT+sGS+smooth number 1-5-10.

$N\backslash m$	10^0	10^1	10^2	10^4	10^5	10^6	10^7	10^8	10^9
Smooth number=1									
131	**60**$^+$, 0.885	**60**$^+$, 0.917	∞, 1.004	∞, 1.109	∞, 1.093	∞, 1.099	∞, 1.141	∞, 1.149	∞, 1.032
451	∞, 0.968	∞, 1.004	∞ 1.041	∞, 1.097	∞, 1.098	∞, 1.111	∞, 1.095	∞, 1.136	∞, 1.179
1667	∞, 0.992	∞, 1.029	∞, 1.055	∞, 1.078	∞, 1.135	∞, 1.107	∞, 1.143	∞, 1.134	∞, 1.179
Smooth number=5									
131	**60**$^+$, 0.885	**60**$^+$, 0.917	∞, 1.004	∞, 1.109	∞, 1.093	∞, 1.099	∞, 1.141	∞, 1.149	∞, 1.032
451	**60**$^+$, 0.761	**60**$^+$, 0.868	**60**$^+$, 0.970	∞, 1.098	∞, 1.137	∞, 1.119	∞, 1.128	∞, 1.169	∞, 1.195
1667	**60**$^+$, 0.855	∞, 0.952	∞, 1.029	∞, 1.039	∞, 1.079	∞, 1.120	∞, 1.182	∞, 1.183	∞, 1.191
Smooth number=10									
131	**60**$^+$, 0.885	**60**$^+$, 0.917	∞, 1.004	∞, 1.109	∞, 1.093	∞, 1.099	∞, 1.141	∞, 1.149	∞, 1.032
451	**41**, 0.671	**60**$^+$, 0.775	**60**$^+$, 0.900	∞, 1.060	∞, 1.141	∞, 1.141	∞, 1.144	∞, 1.178	∞, 1.194
1667	**38**, 0.648	**60**$^+$, 0.767	**60**$^+$, 0.913	∞, 1.055	∞, 1.030	∞, 1.098	∞, 1.117	∞, 1.171	∞, 1.218

Bold characters indicate iteration counts and the number of DOF in the linear system.

Table V. Two-islands case: AGKS+HCT+sGS+smooth number 1-5-10.

$N\backslash m$	10^0	10^1	10^2	10^3	10^4	10^5	10^7	10^9	10^{10}
Smooth number=1									
131	**21**, 0.495	**18**, 0.455	**12**, 0.266	**8**, 0.144	**6**, 0.046	**4**, 0.016	**3**, 0.009	**3**, 0.002	**3**, 0.001
451	**49**, 0.754	**36**, 0.674	**19**, 0.478	**11**, 0.261	**8**, 0.165	**8**, 0.166	**9**, 0.209	**8**, 0.160	**8**, 0.162
1667	**60**$^+$, 0.890	**60**$^+$,0.841	**36**, 0.680	**18**, 0.459	**13**, 0.315	**13**, 0.336	**13**, 0.315	**13**, 0.314	**13**, 0.316
Smooth number=5									
131	**21**, 0.495	**18**, 0.455	**12**, 0.266	**8**, 0.144	**6**, 0.046	**4**, 0.016	**3**, 0.009	**3**, 0.002	**3**, 0.001
451	**42**, 0.717	**32**, 0.625	**17**, 0.436	**10**, 0.215	**6**, 0.074	**5**, 0.057	**4**, 0.004	**4**, 0.001	**3**, 0.003
1667	**60**$^+$, 0.867	**54**, 0.772	**26**, 0.577	**14**, 0.311	**8**, 0.133	**6**, 0.050	**4**, 0.018	**4**, 0.010	**4**, 0.011
Smooth number=10									
131	**21**, 0.495	**18**, 0.455	**12**, 0.266	**8**, 0.144	**6**, 0.046	**4**, 0.016	**3**, 0.009	**3**, 0.002	**3**, 0.001
451	**42**, 0.717	**32**, 0.625	**17**, 0.436	**10**, 0.215	**6**, 0.074	**5**, 0.057	**4**, 0.004	**4**, 0.001	**3**, 0.003
1667	**60**$^+$, 0.866	**54**, 0.769	**26**, 0.576	**14**, 0.311	**8**, 0.133	**6**, 0.041	**4**, 0.007	**4**, 0.004	**4**, 0.006

Bold characters indicate iteration counts and the number of DOF in the linear system.

Owing to Shermann–Woodbury–Morrison formula, the inversion of S_∞ and $S(m)$ requires the inversions of 3×3 and $n_{\mathrm{H}}\times n_{\mathrm{H}}$ matrices.[‡] Therefore, the LRP clearly yields a computational advantage. By exploiting the fact that S_∞ in (1) is only an LRP of K_{LL}, we can build robust preconditioners for S_∞ in (32) via standard multigrid preconditioners. Equation (1) implies that

$$S_\infty = K_{\mathrm{LL}} - v\eta^{-1}v^{\mathrm{T}},$$

where $v := K_{\mathrm{LH}}\mathrm{e}_{\mathrm{H}}$. M_{HH} and M_{LL} denote the standard multigrid $V(s,s)$-cycles for K_{HH} and K_{LL}, respectively. We can construct an efficient and robust preconditioner $\tilde{S}^{-1}$ for S_∞ using the Sherman–Morrison–Woodbury formula, i.e.

$$\tilde{S}^{-1} := M_{\mathrm{LL}} + M_{\mathrm{LL}}v(\eta - v^{\mathrm{T}}M_{\mathrm{LL}}v)^{-1}v^{\mathrm{T}}M_{\mathrm{LL}}. \tag{42}$$

[‡]Let $T_\infty := \eta - v^{\mathrm{t}}K_{\mathrm{LL}}^{-1}v$ and $T(m) := K_{\mathrm{HH}} - K_{\mathrm{LH}}^{\mathrm{t}}K_{\mathrm{LL}}^{-1}K_{\mathrm{LH}}$. The inversions yield the following operations respectively:

$$S_\infty^{-1} = K_{\mathrm{LL}}^{-1} + K_{\mathrm{LL}}^{-1}vT_\infty^{-1}v^{\mathrm{t}}K_{\mathrm{LL}}^{-1},$$

$$S(m)^{-1} = K_{\mathrm{LL}}^{-1} + K_{\mathrm{LL}}^{-1}K_{\mathrm{LH}}T(m)^{-1}K_{\mathrm{LH}}^{\mathrm{t}}K_{\mathrm{LL}}^{-1}.$$

T_∞ is of size 3×3 (in the case of a single island), independent of n_{H} and m, whereas $T(m)$ is of size $n_{\mathrm{H}}\times n_{\mathrm{H}}$, dense, and depends on m.

DOI: 10.1002/nla

Note also that we can precompute and store $M_{\mathrm{LL}}v$ during the setup phase. This means that we only need to apply the multigrid $V(s,s)$-cycle M_{LL} once per iteration. Therefore, the following practical version of preconditioner (32) is used in the implementation:

$$\tilde{B}_{\mathrm{AGKS}} := \begin{bmatrix} I_{\mathrm{HH}} & -K_{\mathrm{HH}}^{\infty\dagger} K_{\mathrm{HL}} \\ 0 & I_{\mathrm{LL}} \end{bmatrix} \begin{bmatrix} M_{\mathrm{HH}} & 0 \\ 0 & \tilde{S}^{-1} \end{bmatrix} \begin{bmatrix} I_{\mathrm{HH}} & 0 \\ -K_{\mathrm{LH}} K_{\mathrm{HH}}^{\infty} & I_{\mathrm{LL}} \end{bmatrix}. \tag{43}$$

We construct two different multilevel hierarchies for multigrid preconditioners M_{HH} in (43) and M_{LL} in (42) for DOF corresponding to Ω_{H} and Ω_{L}, respectively. For prolongation, linear interpolation is used as in [5]. The prolongation matrices P_{HH} and P_{LL} are extracted from the prolongation matrix for whole domain Ω in the following fashion (11):

$$P = \begin{bmatrix} P_{\mathrm{HH}} & P_{\mathrm{HL}} \\ P_{\mathrm{LH}} & P_{\mathrm{LL}} \end{bmatrix}.$$

As emphasized in our preceding paper [1], AGKS can be used purely as an algebraic preconditioner. Therefore, the standard multigrid preconditioner constraint that the coarsest-level mesh resolves the boundary of the island is automatically eliminated. However, for a fair comparison, we enforce the coarsest-level mesh to have that property.

We do not observe convergence improvement when a subdomain deflation strategy based on the smallest eigenvalues is used as in the diffusion equation case [2]. The eigenvectors of the Neumann matrix, e_{H} in (16), cannot approximate the eigenvectors corresponding to the smallest eigenvalues of K_{HH} which are of $\mathcal{O}(1)$ (see Figure 2) since the remainder matrix R in (15) is of $\mathcal{O}(10^4)$. Therefore, a deflation strategy utilizing e_{H} will not necessarily guarantee deflation of the smallest eigenvalues of K_{HH} in the biharmonic case.

We have studied three experiment cases: a square island, an L-shaped island, and two islands (two triangle islands with different coefficient values). With these experiments, we obtain the following results regarding the effect of the number of smoothing iterations on convergence behavior. We do not show the results of MG performance for the two-island case. This is because there is a contrast between the coefficients, and MG fails to converge for any m. For the other two cases, the convergence of MG heavily depends on m and the number of smoothing iterations, i.e. for small m, the more the smoothing iteration, the faster the convergence; see Tables II and IV. However, if the coefficient m is bigger than 10^1, the MG method fails to converge independent of the smoothing number.

Throughout the AGKS experiments, we observe different behaviors of convergence. First of all, for the single square island case, AGKS requires more than one smoothing iteration for convergence; see Table I. The choice of five smoothing iterations is sufficient for AGKS to reach h-robustness and its peak performance for $m > 10^5$. For the L-shaped island case, m-robustness is obtained for smoothing number 1. When the smoothing number is increased to 10, h- and m-robustness are obtained simultaneously; see Table III.

To test the performance of the AGKS preconditioner for the third case, i.e. the case of two islands with different coefficients, we fix the coefficient of one of the islands to 10^9, and devise a coefficient parameter for the second island. We observe that AGKS preconditioner enjoys m robustness even when the smoothing number is one. Moreover, when we set the smoothing number to 5 we obtain that the AGKS preconditioner converges in a few iterations for large m and is h robust. In fact, as it can be seen from Table V, for the same problem size, the AGKS preconditioner demonstrates the best performance for the two-island case.

Hence, when the smoothing number is set to be greater than 10, we can conclude that the AGKS preconditioner clearly enjoys h-robustness for sufficiently large m values independently of the shape or the number of the islands. In contrast, MG is not h-robust regardless of the m value and the smoothing number. MG is totally ineffective as the problem size increases.

Finally, we report the m-robustness results. The loss of m-robustness of MG can be observed consistently for all m values while the AGKS preconditioner becomes more effective with increasing m and reaches its peak performance by maintaining an optimal iteration count for all $m \geqslant 10^5$. This

DOI: 10.1002/nla

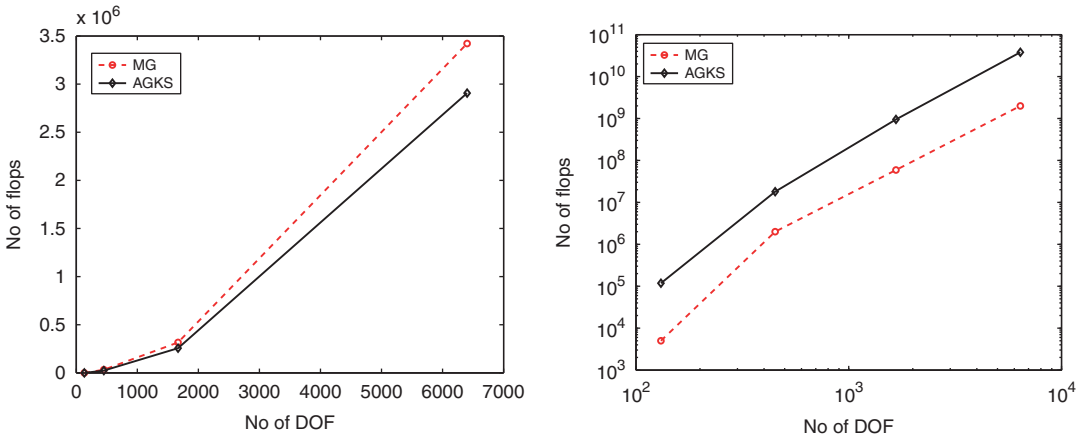

Figure 4. (Left) Flop counts for the enforcement of variational conditions. (Right) Flop counts for a single iteration of the preconditioners.

indicates that $m \geqslant 10^5$ corresponds to the asymptotic regime. Even increasing the m value from 10^2 to 10^3 reduces the iteration count significantly, a clear sign of close proximity to the asymptotic regime. In addition, the AGKS outperforms MG even for $m = 1$. Consequently, we infer that AGKS is m-robust.

We conclude the numerical experiments by reporting the cost of each preconditioner. For variational conditions, the decoupling of $K_{\mathrm{HH}}(m)$ and S^{∞} in (32) causes the AGKS preconditioner to be cheaper than MG, see the flop counts in Figure 4. When the size of the highly bending region grows, the enforcement of the variational conditions of the AGKS preconditioner becomes even less costly than that of the MG preconditioner.

Finally, we report the cost per iteration for the AGKS and MG $V(1, 1)$-cycle preconditioners. The AGKS preconditioner in (32) requires inversions of two blocks: $K_{\mathrm{HH}}(m)$ and S^{∞} corresponding to highly and lowly bending regions, respectively. Therefore, for each iteration of AGKS preconditioner, we utilize a full MG method for each block separately. This is exactly the setup that MG methods are known to be highly effective because each block corresponds to a discretization of the Laplace equation with homogeneous coefficients. Therefore, one iteration of the AGKS preconditioner is roughly 20 times more costly than that of the MG preconditioner; see the flop counts in Figure 4. This additional cost is worthy because after the smoothing number is set to be 5, the AGKS preconditioner results in convergence in a few iterations for large values of m, whereas, no matter what the smoothing number is, the MG preconditioner results in a consistent failure.

7. GENERALIZATION TO ELLIPTIC PDES OF ORDER $2k$

In essence, the biharmonic plate equation preconditioner is an extension of the construction for the diffusion equation. It is possible to generalize this construction to a family of elliptic PDEs of order $2k, k > 2$. We present how to obtain LRPs from associated bilinear forms. We choose a different perspective than the one in Section 3. We start with a canonical bilinear form and show the modification it needs to go through in order to construct LRPs.

Let the generalized problem be stated as follows: Find $u \in H_0^k(\Omega)$ such that

$$T_k u := (-1)^k \nabla^k (\alpha_k \nabla^k u) = f \quad \text{in } \Omega. \tag{44}$$

DOI: 10.1002/nla

The straightforward bilinear form associated with (44) is obtained by the application of Green's formula k times:

$$\int_\Omega \nabla^k(\alpha_k \nabla^k u)v \, \mathrm{d}x = \int_\Omega \alpha_k \nabla^k u \nabla^k v \, \mathrm{d}x + \text{boundary terms}. \tag{45}$$

Then, we define a bilinear form corresponding to (44) which can be seen as a *generalization* of the *canonical* bilinear form in (7):

$$\tilde{a}_k(u, v) := \int_\Omega \alpha_k \nabla^k u \nabla^k v \, \mathrm{d}x. \tag{46}$$

Without modification, $\tilde{a}_k(\cdot, \cdot)$ cannot lead to LRPs because $\tilde{a}_k(v, v)$ is not $H_0^k(\Omega)$-coercive. This is due to the fact that $\tilde{a}_k(v, v) = 0$ for $v \in \mathscr{P}_{k-1} \cap H_0^k(\Omega)$. Hence, the stiffness matrix induced by (46) has a large kernel involving elements from $\mathscr{P}_{k-1}^h \cap V^h$ which indicates that extraction of a Neumann matrix with a low-dimensional kernel is impossible. In order to overcome this complication, we utilize a modified bilinear form:

$$a_k(u, v) = \tilde{a}_k(u, v) + (1 - \sigma_k)\hat{a}_k(u, v).$$

The bilinear form should maintain the following essential properties:

1. $H_0^k(\Omega)$-coercive.
2. $V_{\mathscr{P}_{k-1}(\Omega)}$-coercive.
3. Corresponds to a strong formulation giving $T_k u$ in (44) precisely,

where $V_{\mathscr{P}_{k-1}(\Omega)}$ is a closed subspace such that $V_{\mathscr{P}_{k-1}}(\Omega) \cap \mathscr{P}_{k-1} = \emptyset$ and $\mathscr{P}_{k-1}$ denotes the set of polynomials of degree at most $k-1$.

The above properties (1) and (2) will be immediately satisfied if the generalization of (13) holds for the modified bilinear form:

$$a_k(v, v) \geqslant c_k |v|^2_{H^k(\Omega)}. \tag{47}$$

A similar construction of the *Neumann* matrix can be immediately generalized as follows:

$$\langle \mathscr{N}_{\mathrm{HH}}^{(k)} \underline{\phi}^h, \underline{\psi}^h \rangle := a_k(\phi_{\mathrm{H}}^h, \psi_{\mathrm{H}}^h).$$

The LRPs arise from the following decomposition of $K_{\mathrm{HH}}^{(k)}(m)$:

$$K_{\mathrm{HH}}^{(k)}(m) = m\mathscr{N}_{\mathrm{HH}}^{(k)} + R^{(k)}, \quad (K_{\mathrm{HH}}^{(k)}(m))^{-1} = \mathrm{e}_{\mathrm{H}}^{(k)} \eta^{(k)^{-1}} \mathrm{e}_{\mathrm{H}}^{(k)^{\mathrm{t}}} + \mathscr{O}(m^{-1}),$$

where $\eta^{(k)} := \mathrm{e}_{\mathrm{H}}^{(k)^{\mathrm{t}}} K_{\mathrm{HH}}^{(k)} \mathrm{e}_{\mathrm{H}}^{(k)}$. LRP is produced by $\mathrm{e}_{\mathrm{H}}^{(k)} \in \mathscr{P}_{k-1}^h$ because the rank is equal to the cardinality of the basis polynomials in $\mathscr{P}_{k-1}^h$.

$$\ker \mathscr{N}_{\mathrm{HH}}^{(k)} = \mathscr{P}_{k-1}^h|_{\overline{\Omega}_{\mathrm{H}}}.$$

Owing to (8), $a_2(\cdot, \cdot)$ in (5) corresponds to the strong formulation of T_2 exactly. Let us denote the strong formulation to which $a_k(\cdot, \cdot)$ corresponds by $\hat{T}_k$. We have $\hat{T}_k = T_k$, $k = 1, 2$, for the high-contrast diffusion and biharmonic plate equations, respectively:

$$a_1(v, v) := (\nabla v, \alpha_1 \nabla v),$$
$$a_2(v, v) := \sigma_2(\nabla^2 v, \alpha_2 \nabla^2 v) + \alpha_2(1 - \sigma_2)|v|^2_{H^2(\Omega)}.$$

DOI: 10.1002/nla

However, for general k, $a_k(\cdot,\cdot)$ may not correspond to T_k. In addition, one may need more general boundary conditions if similar zero contributions in (8) can be obtained for general k. Further research is needed to see if such boundary conditions are physical. Currently, it is also unclear for which applications such general PDEs can be used. However, there are interesting invariance theory implications when one employs bilinear forms corresponding to rotationally invariant functions compatible to energy definition in (4). This allows a generalization of the energy notion and may be the subject for future research. For further information, we list the relevant bilinear forms that are composed of rotationally invariant functions derived by the utilization of invariance theory.

$$a_3(v,v) := \sigma_3(\nabla^3 v, \alpha_3\nabla^3 v) + \alpha_3(1-\sigma_3)|v|^2_{H^3(\Omega)},$$

$$a_4(v,v) := \sigma_4(\nabla^4 v, \alpha_4\nabla^4 v) + \alpha_4(1-\sigma_4)|v|^2_{H^4(\Omega)} + \alpha_4\gamma_4|\nabla^2 v|^2_{H^2(\Omega)}.$$

Note that the above bilinear forms satisfy (47).

ACKNOWLEDGEMENTS

This work is supported by NSF under grant number DMS-1016190.

REFERENCES

1. Aksoylu B, Graham IG, Klie H, Scheichl R. Towards a rigorously justified algebraic preconditioner for high-contrast diffusion problems. *Computing and Visualization in Science* 2008; **11**:319–331. DOI: 10.1007/s00791-008-0105-1.
2. Aksoylu B, Yeter Z. Robust multigrid preconditioners for cell-centered finite volume discretization of the high-contrast diffusion equation. *Computing and Visualization in Science* 2010; **13**:229–245. DOI: 10.1007/s00791-010-0140-6.
3. Mihajlović M, Silvester D. Efficient parallel solvers for the biharmonic equation. *Parallel Computing* 2004; **30**:35–55.
4. Zhang X. Multilevel Schwarz methods for the biharmonic Dirichlet problem. *SIAM Journal on Scientific Computing* 1994; **15**:621–644.
5. Braess D, Peisker P. A conjugate gradient method and a multigrid algorithm for Morley's finite element approximation of the biharmonic equation. *Numerische Mathematik* 1987; **50**:567–586.
6. Hanisch MR. Multigrid preconditioning for the biharmonic Dirichlet problem. *SIAM Journal on Numerical Analysis* 1993; **30**:184–214.
7. Mihajlovic M, Silvester D. A black-box multigrid preconditioner for the biharmonic equation. *BIT Numerical Mathematics* 2004; **44**:151–163.
8. Maes J, Bultheel A. A hierarchical basis preconditioner for the biharmonic equation on the sphere. *IMA Journal of Numerical Analysis* 2006; **26**:563–583.
9. Oswald P. Hierarchical conforming finite element methods for the biharmonic equation. *SIAM Journal on Numerical Analysis* 1992; **29**:1610–1625.
10. Oswald P. Multilevel preconditioners for discretizations of the biharmonic equation by rectangular finite elements. *Numerical Linear Algebra with Applications* 1995; **2**:487–505.
11. Mayo A. The fast solution of Poisson's and the biharmonic equations on irregular regions. *SIAM Journal on Numerical Analysis* 1984; **21**:285–299.
12. Mayo A, Greenbaum A. Fast parallel iterative solution of Poisson's and the biharmonic equations on irregular regions. *SIAM Journal on Scientific and Statistical Computing* 1992; **13**:101–118.
13. Dang QA. Iterative method for solving the Neumann boundary value problem for biharmonic type equation. *Journal of Computational and Applied Mathematics* 2006; **196**:643–643.
14. Marcinkowski L. An additive Schwarz method for mortar finite element discretizations of the 4th order elliptic problem in 2D. *Electronic Transactions on Numerical Analysis* 2007; **26**:34–54.
15. Wang TS. A Hermite cubic immersed finite element space for beam design problems. *Master Thesis*, Department of Mathematics, Virginia Polytechnic Institute and State University, 2005.
16. Pozrikidis C. *Introduction to Finite and Spectral Element Methods using MATLAB*. Chapman& Hall/CRC: Boca Raton, FL, 2005.
17. Manolis GD, Rangelov TV, Shaw RP. The non-homogeneous biharmonic plate equation: fundamental solutions. *International Journal of Solids and Structures* 2003; **40**:5753–5767.
18. Miller KL, Horgan CO. End effects for plane deformations of an elastic anisotropic semi-infinite strip. *Journal of Elasticity* 1995; **38**:261–316.
19. Grossi RO. On the existence of weak solutions in the study of anisotropic plates. *Journal of Sound and Vibration* 2001; **242**:542–552.

20. Bakhvalov NS, Knyazev AV. A new iterative algorithm for solving problems of the fictitious flow method for elliptic equations. *Soviet Mathematics Doklady* 1990; **41**:481–485.
21. Knyazev A, Widlund O. Lavrentiev regularization + Ritz approximation = uniform finite element error estimates for differential equations with rough coefficients. *Mathematics of Computation* 2003; **72**:17–40.
22. Aksoylu B, Beyer HR. Results on the diffusion equation with rough coefficients. *SIAM Journal on Mathematical Analysis* 2010; **42**:406–426.
23. Aksoylu B, Beyer HR. On the characterization of the asymptotic cases of the diffusion equation with rough coefficients and applications to preconditioning. *Numerical Functional Analysis and Optimization* 2009; **30**: 405–420.
24. Ciarlet PG. *The Finite Element Method for Elliptic Problems*. Classics in Applied Mathematics. SIAM: Philadelphia, PA, 2002.
25. Aksoylu B, Klie H. A family of physics-based preconditioners for solving elliptic equations on highly heterogeneous media. *Applied Numerical Mathematics* 2009; **59**:1159–1186. DOI: 10.1016/j.apnum.2008.06.002.
26. Graham IG, Hagger MJ. Unstructured additive Schwarz-conjugate gradient method for elliptic problems with highly discontinuous coefficients. *SIAM Journal on Scientific Computing* 1999; **20**:2041–2066.
27. Clough RW, Tocher JL. Finite element stiffness matrices for analysis of plates in bending. *Proceedings of the Conference on Matrix Methods in Structural Mechanics*, Wright Patterson A.F.B., Ohio, 1965.
28. Kato T. *A Short Introduction to Perturbation Theory for Linear Operators*. Springer: Berlin, Germany, 1982.
29. Watkins DS. *Fundamentals of Matrix Computations* (2nd edn). Wiley-Interscience: New York, 2002.
30. Aksoylu B, Bond S, Holst M. An odyssey into local refinement and multilevel preconditioning III: implementation and numerical experiments. *SIAM Journal on Scientific Computing* 2003; **25**:478–498.

DOI: 10.1002/nla